

Raman-Heterodyne Study of the Hyperfine Interaction of the Optically-Excited State 5D_0 of $\text{Eu}^{3+}:\text{Y}_2\text{SiO}_5$

Yu Ma,^{1,2} Zong-Quan Zhou,^{1,2,*} Yong-Jian Han,^{1,2} Chao Liu,^{1,2} Tian-Shu Yang,^{1,2} Tao Tu,^{1,2} Yi-Xin Xiao,^{1,2} Peng-Jun Liang,^{1,2} Pei-Yun Li,^{1,2} Yi-Lin Hua,^{1,2} Xiao Liu,^{1,2} Zong-Feng Li,^{1,2} Jun Hu,^{1,2} Xue Li,^{1,2} Chuan-Feng Li,^{1,2,†} and Guang-Can Guo^{1,2}

¹CAS Key Laboratory of Quantum Information, University of Science and Technology of China, Hefei, 230026, P.R.China

²Synergetic Innovation Center of Quantum Information and Quantum Physics, University of Science and Technology of China, Hefei, 230026, P.R.China

(Dated: July 19, 2022)

The spin coherence time of $^{151}\text{Eu}^{3+}$ which substitutes the yttrium at site 1 in Y_2SiO_5 crystal has been extended to 6 hours in a recent work [*Nature* **517**, 177 (2015)]. To make this long-lived spin coherence useful for optical quantum memory applications, we experimentally characterize the hyperfine interaction of the optically-excited state 5D_0 using Raman-heterodyne-detected nuclear magnetic resonance. The effective spin Hamiltonians for excited and ground state are fitted based on the experimental spectra obtained in 200 magnetic fields with various orientations. To show the correctness of the fitted parameters and potential application in quantum memory protocols, we also characterize the ground-state hyperfine interaction and predict the critical magnetic field which produces the 6-hour-long coherence time. The complete energy level structure for both the 7F_0 ground state and 5D_0 excited state at the critical magnetic field are obtained. These results enable the design of quantum memory protocols and the optimization of optical pumping strategy for realization of photonic quantum memory with hour-long lifetime.

I. INTRODUCTION

As an essential component in quantum repeater scheme,¹ quantum memory is the core element for the construction of large-scale quantum network. Experiments have been performed in many systems such as atomic gases,²⁻⁴ single atom,⁵ molecular gases⁶ and rare-earth ions doped in a crystal (REIC).

It is noteworthy that REIC approach has drawn great interest, and proven to be a promising candidate for quantum memory with high efficiency,⁷ high fidelity,^{8,9} broadband operation¹⁰ and long lifetime¹¹ over the last decade. Among all kinds of REICs, europium ions doped in yttrium orthosilicate ($\text{Eu}^{3+}:\text{Y}_2\text{SiO}_5$) are considered suitable for the realization of long-term quantum storage due to its extremely long relaxation time¹² (22 days) in the ground state. Recently, the spin coherence time for $^{151}\text{Eu}^{3+}$ has been extended to 6 hours in Y_2SiO_5 crystal using a carefully aligned magnetic field and dynamical decoupling.¹³ The unprecedented long coherence time could enable the construction of portable quantum hard drives for entanglement distribution.¹⁴

The knowledge of hyperfine structure is the prerequisite for the design of optical pumping strategy and memory protocols.¹⁵⁻¹⁷ To obtain the information of hyperfine structure of non-Kramers ions, such as Eu^{3+} that interests us, spectral hole burning technique¹⁸⁻²¹ and Raman heterodyne method²²⁻²⁵ are two powerful tools towards high spectral resolution. Conventional nuclear magnetic resonance (NMR) and nuclear quadrupole resonance (NQR) of Eu^{3+} in solids have not been successful due to its small nuclear quadrupole moment,²⁶ while Raman heterodyne method enables high-resolution measurements of the hyperfine interaction with high signal-

to-noise ratio (SNR).^{22,23}

In this work, a brief review is given on the theory of hyperfine interactions for REIC in Sec. II. The experimental setup for Raman-heterodyne-detected NMR is described in Sec. III A. The NMR spectra of the excited state 5D_0 and ground state 7F_0 of $^{151}\text{Eu}^{3+}$ in Y_2SiO_5 are measured in a vector magnetic field of 800 Gauss. The orientation of the field is rotated and 200 independent NMR spectra are obtained shown in Sec. III B. Based on the measured spectra, the effective spin Hamiltonians for 5D_0 and 7F_0 are determined. The fitting procedure and results are presented in Sec. III C. The hyperfine structure in a critical magnetic field can be predicted using the fitted Hamiltonians, which is presented in Sec. III D.

II. THEORY OF HYPERFINE INTERACTIONS FOR REIC

The theory for hyperfine interaction of rare-earth ion doped in crystal has been investigated and elaborated in previous publications.^{21,24,25,27} Here we give a brief review.

The Hamiltonian for 4f electron and nucleus of rare-earth ion has the form

$$H = H_{FI} + H_{CF} + H_{HF} + H_Q + H_z + H_Z. \quad (1)$$

These six terms represent the free ion, crystal field, hyperfine, nuclear quadrupole, electronic Zeeman and nuclear Zeeman Hamiltonians, respectively. The free ion and crystal field terms determine the electronic energy levels and optical transitions. Due to the fact that there is no net electron spin or orbital angular momentum in $\text{Eu}^{3+}:\text{Y}_2\text{SiO}_5$, the other four terms are small enough

to be treated as a perturbation for the electronic state. Using second order perturbation theory and discarding the perturbation term that does not influence the hyperfine energy level, we can obtain the effective spin Hamiltonian^{24,25}

$$H = B \cdot M \cdot I + I \cdot Q \cdot I, \quad (2)$$

where B is the external magnetic field. M and Q are the effective Zeeman and quadrupole tensors for rare-earth ion. I is the nuclear spin operator, which for spin-5/2 nuclei like Eu^{3+} can be parameterized as three 6×6 matrices. The parameterization is presented in III C.

Y_2SiO_5 has a symmetry which can be described by C_{2h}^6 space group. Yttriums occupy two sites in the crystal. Eu^{3+} as a dopant substituting yttrium also occupies two sites. These two sites can be optically distinguishable, which absorb at 580.039 nm and 580.211 nm for site 1 and 2 respectively.²⁸ Each site can be divided into two magnetically inequivalent sets, related to each other by the crystal C_2 axis and an inversion. Here we measure the excited hyperfine structure of $^{151}\text{Eu}^{3+}$ at site 1.

Due to the C_2 symmetry, two sets of Eu^{3+} should be described by different M and Q tensors. Each can be transformed into the other by a π -rotation operation according to the C_2 axis.

III. EXPERIMENT

A. Raman heterodyne spectroscopy

Raman heterodyne spectroscopy, an RF-optical double-resonance technique, has been proven to be a useful tool for NMR measurements for $^7\text{F}_0$ ground state of $^{151}\text{Eu}^{3+}$ ions.²⁴ Here we present the complete measurements on both $^5\text{D}_0$ and $^7\text{F}_0$ state.

The hyperfine structure and experiment setup in a small magnetic field are shown in Fig. 1. As an example, we first introduce the strategy for detection of the $|\pm 1/2\rangle_e \leftrightarrow |\pm 3/2\rangle_e$ transition in the $^5\text{D}_0$ excited state. With a laser resonant with $|\pm 3/2\rangle_g \leftrightarrow |\pm 1/2\rangle_e$ transition at frequency ω_L shone on the crystal, an RF field generated by a local oscillator simultaneously drive the $|\pm 1/2\rangle_e \leftrightarrow |\pm 3/2\rangle_e$ transition at frequency ω_{RF} . A scattered light wave at frequency $\omega_L + \omega_{RF}$ is stimulatedly emitted, co-propagating and beating with the transmitted light at ω_L . A beat signal at ω_{RF} is captured on the detector and demodulated by the RF local oscillator as long as the Raman process has happened.

The laser source is a frequency-doubled semiconductor laser with a linewidth well below 10 kHz. The probe beam propagates along the crystal C_2 axis and has a beam diameter of approximately $50 \mu\text{m}$ inside the crystal. The transmitted light is coupled into a single-mode fiber and detected with a photodetector. A 7-turn coil is wrapped around the crystal to produce the RF field along the C_2 axis.

The pump beam that sweeps the frequency around the $|\pm 1/2\rangle_g \leftrightarrow |\pm 3/2\rangle_e$ is employed in the measurements of $|\pm 1/2\rangle_e \leftrightarrow |\pm 3/2\rangle_e$. The SNR with the pump beam is significantly better than that without pump. There are two reasons that may explain this phenomenon. One is the linear relationship between NMR signal and the population difference between the hyperfine levels,²² which can be increased by the pump light. The other reason is similar to what is mentioned in Ref. 24, where J. J. Longdell *et al.* did not find the Raman signal without a pump light. Here, if the signal light is incident without pump, all of the ground states contribute to the Raman signal. A repump light can break the symmetry, further increase the signal.

The power of the pump light is approximately 7 mW before entering the crystal. The pump beam has a diameter of approximately two times of that for the probe beam. The probe and pump beam overlap inside the crystal, with a small angle between their propagating directions.

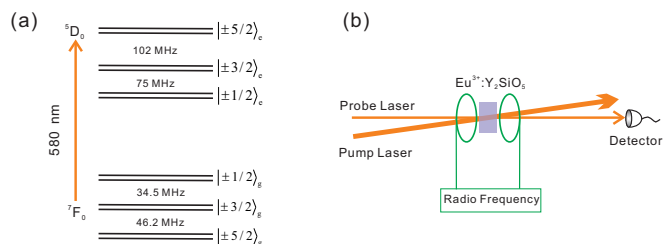


FIG. 1. (Color online) (a) The hyperfine structure of the ground state $^7\text{F}_0$ and excited state $^5\text{D}_0$ of $^{151}\text{Eu}^{3+}$ at site 1 of Y_2SiO_5 in a small magnetic field. (b) Experimental setup for Raman-heterodyne-detected NMR of $\text{Eu}^{3+}:\text{Y}_2\text{SiO}_5$. A probe laser is incident on the crystal placed inside a cryostat, while an RF field delivered by a 7-turn coil drives the hyperfine transitions. A pump laser is employed to create a population difference between two hyperfine states. The photodetector captures the beat signal produced by the transmitted light and the scattered light.

B. Spectrum measurements

The $\text{Eu}^{3+}:\text{Y}_2\text{SiO}_5$ crystal used in this experiment has a size of $4 \times 3 \times 10 \text{ mm}$, cut along the three crystal axes D_1 , D_2 and b . The impurity density of europium ion is 0.1%. The crystal is placed inside a cryostat and cooled to about 3.5 K for the spectrum measurements.

In order to obtain the information of hyperfine structure of Eu^{3+} in magnetic field, a DC magnetic field of 800 Gauss is applied to the crystal to split the degenerate hyperfine energy levels. We follow the similar experiment performed for ground state $^7\text{F}_0$,^{24,25} rotating the direc-

tion of the magnetic field in a spherical pattern

$$\begin{cases} B_x = B_0 \sqrt{1-t^2} \cos(6\pi t) \\ B_y = B_0 \sqrt{1-t^2} \sin(6\pi t) \\ B_z = B_0 t \end{cases} \quad (3)$$

in which $t \in [-1, 1]$.

The formula is given in laboratory coordinate system, with three axes corresponding to the field directions of XYZ coils. The crystal is placed in inside the XYZ coils by hand, so that the crystal coordinate system $[D_1, D_2, b]$ has a small misalignment with the laboratory system. This misalignment does not bring extra error to the measurement because it can be fitted in the fitting procedure. See the next section for details.

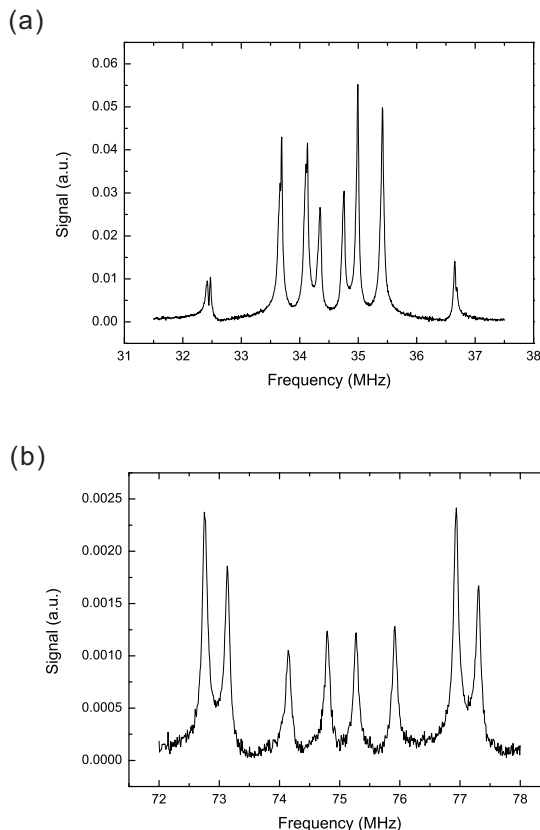


FIG. 2. Two typical Raman-heterodyne spectra for the ground (a) and excited (b) state obtained in No. 68 and No. 55 magnetic field, respectively. Eight peaks can be clearly located with very good SNR for both excited and ground state. Unexpected tiny splittings are observed for $|\pm 1/2\rangle_g \leftrightarrow |\pm 3/2\rangle_g$ transition around 34.5 MHz, which requires more investigations in the future. For fitting procedure, we take the average values of these splitted peaks as a reasonable approximation.

The spectrum acquisition is carried out around 75 MHz and 102 MHz for two excited-state transitions $|\pm 1/2\rangle_e \leftrightarrow |\pm 3/2\rangle_e$ and $|\pm 3/2\rangle_e \leftrightarrow |\pm 5/2\rangle_e$, and 34.5 MHz and 46.2 MHz for two ground-state transitions $|\pm 1/2\rangle_g \leftrightarrow |\pm 3/2\rangle_g$

and $|\pm 3/2\rangle_g \leftrightarrow |\pm 5/2\rangle_g$ respectively in 200 magnetic fields, according to $t \in [-1, 1]$ divided into 200 points. In total, 800 spectra are obtained. Over 1000 averages are taken to reach a good SNR for each excited-state spectrum. For ground state measurements, only 100 averages are taken because of a much better SNR. Two typical spectra for the excited and ground state are presented in Fig. 2. The SNR of the observed spectra is sufficient for determining the parameters of the Hamiltonian.

Unexpected splittings are observed in the $|\pm 1/2\rangle_g \leftrightarrow |\pm 3/2\rangle_g$ transition. Typical examples are the first three peaks and the last one in Fig. 2. The largest splitting we observed is approximately 100 kHz. We also performed the measurements for a 0.01% doped crystal. Although the linewidth for each peak is narrower for the sample with lower impurity density, these superhyperfine splittings still present. It seems that there may exist superhyperfine interaction that the spin Hamiltonian above may be unable to explain. Further studies are required to identify the mechanisms for these splittings. As a reasonable approximation, we take the average value of the positions of those tiny peaks as the actual transition frequency for fitting procedure.

C. Fitting of the Hamiltonian parameters

The parameterization of the effective spin Hamiltonian for 5D_0 state is the same as that used for 7F_0 state.²⁴ Two parameter are required to determine the Q tensor in its principal axis system:

$$\begin{pmatrix} -E & 0 & 0 \\ 0 & E & 0 \\ 0 & 0 & D \end{pmatrix}. \quad (4)$$

Then the Q tensor in the lab coordinate system can be obtained by a rotation characterized by Euler angles, *i. e.*:

$$Q_1 = R(\alpha_Q, \beta_Q, \gamma_Q) \begin{pmatrix} -E & 0 & 0 \\ 0 & E & 0 \\ 0 & 0 & D \end{pmatrix} R^T(\alpha_Q, \beta_Q, \gamma_Q). \quad (5)$$

The footnote 1 denotes one of the two magnetically inequivalent sets. The rotation matrix $R(\alpha, \beta, \gamma)$ can be written in the form:

$$R(\alpha, \beta, \gamma) = \begin{pmatrix} \cos \alpha & -\sin \alpha & 0 \\ \sin \alpha & \cos \alpha & 0 \\ 0 & 0 & 1 \end{pmatrix} \cdot \begin{pmatrix} \cos \beta & 0 & \sin \beta \\ 0 & 1 & 0 \\ -\sin \beta & 0 & \cos \beta \end{pmatrix} \cdot \begin{pmatrix} \cos \gamma & -\sin \gamma & 0 \\ \sin \gamma & \cos \gamma & 0 \\ 0 & 0 & 1 \end{pmatrix}, \quad (6)$$

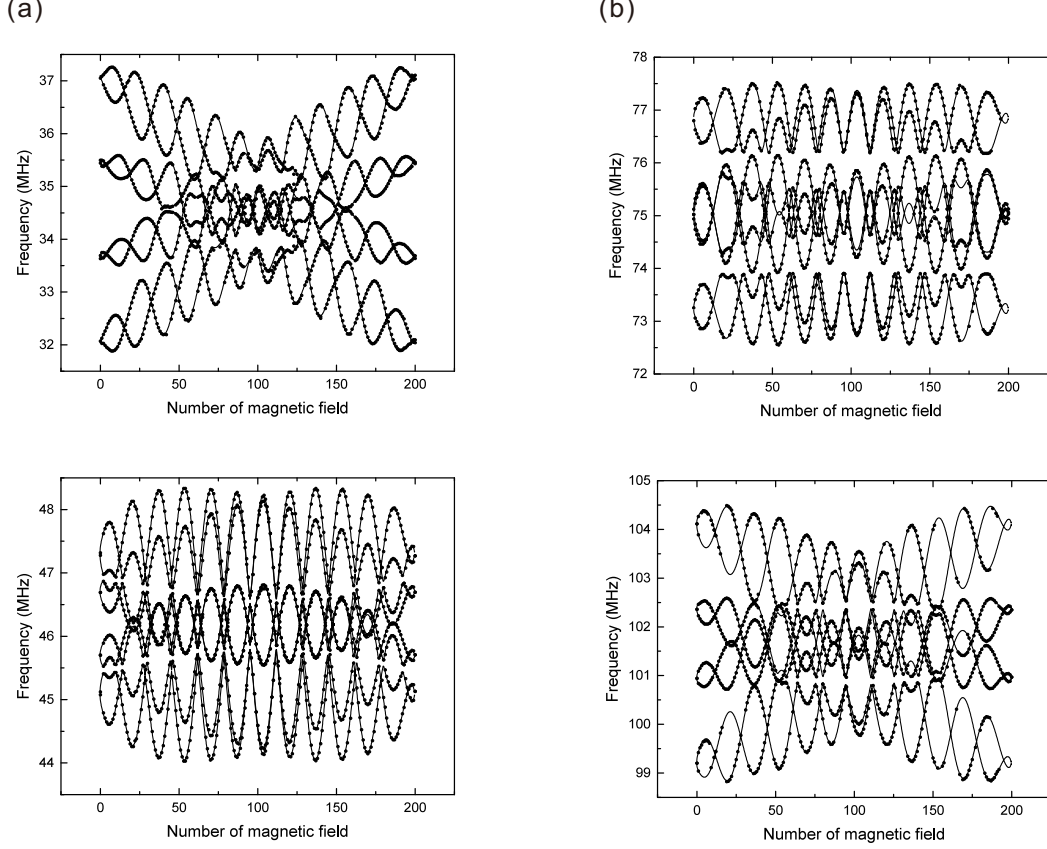


FIG. 3. The experimental spectra and fitting results for the ground-state (a) and excited-state (b) hyperfine transitions in 200 magnetic fields. Dots are the NMR peaks detected in the experiment, and the solid lines represent the predicted position of peaks.

where the footnote Q has been taken away since the rotation matrix has the same form for the M tensor:

$$M_1 = R(\alpha_M, \beta_M, \gamma_M) \begin{pmatrix} g_1 & 0 & 0 \\ 0 & g_2 & 0 \\ 0 & 0 & g_3 \end{pmatrix} R^T(\alpha_M, \beta_M, \gamma_M). \quad (7)$$

M_2 and Q_2 tensors for another set of ions can be easily obtained by a π -rotation operation on M_1 and Q_1 according to the crystal C_2 axis. We assume an azimuthal angle θ and a polar angle ϕ for the direction of the C_2 axis because of the misalignment between lab and crystal system mentioned in the last section. The π -rotation operation can be written in matrix form:²⁹

$$R_\pi(\theta, \phi) = I + 2J(\theta, \phi)J^T(\theta, \phi), \quad (8)$$

where $J(\theta, \phi)$ is the skew symmetric operator:

$$J(\theta, \phi) = \begin{pmatrix} 0 & -\cos\theta & \sin\theta \sin\phi \\ \cos\theta & 0 & -\sin\theta \cos\phi \\ -\sin\theta \sin\phi & \sin\theta \cos\phi & 0 \end{pmatrix}. \quad (9)$$

After the parameterization of the spin Hamiltonian, one can obtain the eigenenergy spectrum by solving the stationary Schrödinger equation, as long as those parameters are assigned with certain values. In the fitting procedure, we first use a random set of values to parameterize the Hamiltonians, then minimize the error between the calculated spectra and the experimental ones by continuously optimizing the parameters.

The error minimization is carried out by computer using simulated annealing algorithm.³⁰ The objective function is set to be the total absolute error of the 800 spectra of both excited and ground hyperfine transitions.

The final fitting results are shown in Fig. 3 and Tab. I. Note that the θ and ϕ are the same for both the excited and ground state since the orientation of the C_2 axis is fixed in the lab system. The final fitting error is reduced to roughly 14 kHz per peak on average, which is comparable to the experimental error and the inhomogeneous broadening. Note that the azimuth angle θ for the crystal C_2 axis is small, which confirms that the crystal coordinate system is approximately aligned with the lab system. The absolute values of the diagonal elements of

TABLE I. Fit results for spin Hamiltonian parameters. θ and ϕ are the same for the excited and ground state because the orientation of the C_2 axis is fixed in the lab system.

	Excited state 5D_0	Ground state 7F_0
α_M (rad)	-1.3878	0.5077
β_M (rad)	1.5647	-1.1289
γ_M (rad)	-1.1985	0.0752
g_1 (MHz/T)	9.5894	11.8015
g_2 (MHz/T)	9.4437	4.7502
g_3 (MHz/T)	10.1885	-5.8266
α_Q (rad)	0.6182	-2.9353
β_Q (rad)	-0.5312	0.8051
γ_Q (rad)	0.0240	-2.3720
E (MHz)	5.8713	-2.7359
D (MHz)	27.1861	-12.3819
θ (rad)	0.0559	
ϕ (rad)	5.7904	

the M and Q tensors, *i. e.* the g -factors, E and D of the ground state 7F_0 are close to the results in Ref. 24.

D. Predictions on the hyperfine structure for Eu^{3+} in high magnetic fields

A straightforward application of the obtained spin Hamiltonians is to predict the hyperfine structure for Eu^{3+} in higher magnetic fields. Here we take the zero first order Zeeman (ZEFOZ) magnetic field employed to realize 6-hour coherence time for example.¹³

ZEFOZ point is a certain magnetic field in which the frequency of considered hyperfine perturbation is extremely insensitive to the magnetic field perturbation. Since the magnetic field noise from the nuclear spin baths are the primary source of decoherence for Eu^{3+} in Y_2SiO_5 , the considered transition should have a extended coherence time at ZEFOZ point. We first search for the ZEFOZ points for $|-3/2\rangle_g \leftrightarrow |+3/2\rangle_g$ using the fitted spin Hamiltonians. One of the ZEFOZ magnetic fields is found at 1.261 Tesla in the direction $[-0.5914, 0.5239, 0.6130]$ in our laboratory system, which is coincident with the experimental results in Ref. 13. The hyperfine structure at this point is shown in Fig. 4. One can find in the figure the 12.46 MHz ZEFOZ transition in the ground state 7F_0 used to realize 6-hour coherence time.

As a matter of fact, the hyperfine structure in any mag-

netic fields can be easily predicted based on the fitted spin Hamiltonians. With known energy level structure, optical pumping strategy can be designed for the current system in any other ZEFOZ magnetic field. A Λ system can

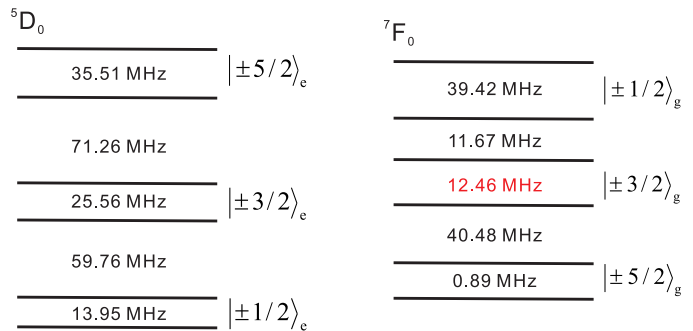


FIG. 4. (Color online) Hyperfine structure of the excited state 5D_0 and ground state 7F_0 of ${}^{151}\text{Eu}^{3+}$ at site 1 in Y_2SiO_5 in a ZEFOZ magnetic field.¹³ The transition with a frequency of 12.46 MHz is extremely insensitive to the magnetic field perturbation.

be well selected within the inhomogeneous broadening and tailored into suitable absorption shape through optical pumping for quantum memory protocols such as electromagnetic induced transparency (EIT),¹⁷ controlled reversible inhomogeneous broadening (CRIB)¹⁶ and atomic frequency comb (AFC).¹⁵

IV. CONCLUSION

By using Raman-heterodyne-detected NMR, the hyperfine interactions in the excited state 5D_0 and ground state 7F_0 of ${}^{151}\text{Eu}^{3+}$ in Y_2SiO_5 are characterized. The effective Hamiltonians for excited and ground state are obtained, based on which we find the ZEFOZ magnetic field in which hour-long coherence of $|-3/2\rangle_g \leftrightarrow |+3/2\rangle_g$ is realized recently.¹³ The hyperfine structure of excited state at this point is predicted, which can find applications in the design of optical pumping strategy for quantum memory protocols. As a matter of fact, more and better ZEFOZ points can be found in higher magnetic fields, and energy levels of Eu^{3+} in those fields can be easily given using the same Hamiltonians.

The method in this work can be generalized to other non-Kramers ions doped in a crystal. Combining our results with ZEFOZ technique and dynamical decoupling sequence, an optical quantum memory with hour-long lifetime may be constructed in the future, which could enable novel methods for long-distance quantum communication.¹⁴

We note that similar results are obtained through optical free induction decay measurement by an independent group.³¹

- * zq'zhou@ustc.edu.cn
† c'li@ustc.edu.cn
- ¹ H. J. Briegel, W. Dur, J. I. Cirac, and P. Zoller, *Physical Review Letters* **81**, 5932 (1998).
 - ² M. D. Lukin, *Reviews of Modern Physics* **75**, 457 (2003).
 - ³ K. S. Choi, H. Deng, J. Laurat, and H. J. Kimble, *Nature* **452**, 67 (2008).
 - ⁴ D. N. Matsukevich and A. Kuzmich, *Science* **306**, 663 (2004).
 - ⁵ H. P. Specht, C. Nolleke, A. Reiserer, M. Uphoff, E. Figueroa, S. Ritter, and G. Rempe, *Nature* **473**, 190 (2011).
 - ⁶ P. Rabl, D. DeMille, J. M. Doyle, M. D. Lukin, R. J. Schoelkopf, and P. Zoller, *Phys Rev Lett* **97**, 033003 (2006).
 - ⁷ M. P. Hedges, J. J. Longdell, Y. Li, and M. J. Sellars, *Nature* **465**, 1052 (2010).
 - ⁸ Z.-Q. Zhou, W.-B. Lin, M. Yang, C.-F. Li, and G.-C. Guo, *Physical Review Letters* **108**, 190505 (2012).
 - ⁹ Z. Q. Zhou, Y. L. Hua, X. Liu, G. Chen, J. S. Xu, Y. J. Han, C. F. Li, and G. C. Guo, *Phys Rev Lett* **115**, 070502 (2015).
 - ¹⁰ E. Saglamyurek, N. Sinclair, J. Jin, J. A. Slater, D. Oblak, F. Bussieres, M. George, R. Ricken, W. Sohler, and W. Titel, *Nature* **469**, 512 (2011).
 - ¹¹ G. Heinze, C. Hubrich, and T. Halfmann, *Physical Review Letters* **111**, 033601 (2013).
 - ¹² F. Konz, Y. Sun, C. W. Thiel, R. L. Cone, R. W. Equall, R. L. Hutcheson, and R. M. Macfarlane, *Physical Review B* **68**, 085109 (2003).
 - ¹³ M. Zhong, M. P. Hedges, R. L. Ahlefeldt, J. G. Bartholomew, S. E. Beavan, S. M. Wittig, J. J. Longdell, and M. J. Sellars, *Nature* **517**, 177 (2015).
 - ¹⁴ J. J. L. Morton and K. Molmer, *Nature* **517**, 153 (2015).
 - ¹⁵ M. Afzelius, I. Usmani, A. Amari, B. Lauritzen, A. Walther, C. Simon, N. Sangouard, J. Minar, H. de Riedmatten, N. Gisin, et al., *Phys Rev Lett* **104**, 040503 (2010).
 - ¹⁶ M. Nilsson and S. Kroll, *Optics Communications* **247**, 393 (2005).
 - ¹⁷ A. V. Turukhin, V. S. Sudarshanam, M. S. Shahriar, J. A. Musser, B. S. Ham, and P. R. Hemmer, *Phys Rev Lett* **88**, 023602 (2001).
 - ¹⁸ A. Arcangeli, M. Lovric, B. Tumino, A. Ferrier, and P. Goldner, *Physical Review B* **89**, 184305 (2014).
 - ¹⁹ B. Lauritzen, N. Timoney, N. Gisin, M. Afzelius, H. de Riedmatten, Y. Sun, R. M. Macfarlane, and R. L. Cone, *Physical Review B* **85**, 115111 (2012).
 - ²⁰ M. Nilsson, L. Rippe, S. Kroll, R. Klieber, and D. Suter, *Physical Review B* **70**, 214116 (2004).
 - ²¹ J. P. D. Martin, M. J. Sellars, P. Tuthill, N. B. Manson, G. Pryde, and T. Dyke, *Journal of Luminescence* **78**, 19 (1998).
 - ²² N. C. Wong, E. S. Kintzer, J. Mlynek, R. G. DeVoe, and R. G. Brewer, *Physical Review B* **28**, 4993 (1983).
 - ²³ J. Mlynek, N. C. Wong, R. G. DeVoe, E. S. Kintzer, and R. G. Brewer, *Physical Review Letters* **50**, 993 (1983).
 - ²⁴ J. J. Longdell, A. L. Alexander, and M. J. Sellars, *Physical Review B* **74**, 195101 (2006).
 - ²⁵ J. J. Longdell, M. J. Sellars, and N. B. Manson, *Physical Review B* **66**, 035101 (2002).
 - ²⁶ G. Liu and B. Jacquier, *Spectroscopic Properties of Rare Earths in Optical Materials* (Springer, Berlin, 2005).
 - ²⁷ A. A. Kaplyanskii and R. M. Macfarlane, eds., *Spectroscopy of Solids Containing Rare Earth Ions* (North-Holland, Amsterdam, 1987).
 - ²⁸ M. J. Thorpe, D. R. Leibrandt, and T. Rosenband, *New Journal of Physics* **15** (2013).
 - ²⁹ C. J. Taylor and D. J. Kriegman, Tech. Rep. 9405, Yale University (1994).
 - ³⁰ S. Kirkpatrick, J. Gelatt, C. D., and M. P. Vecchi, *Science* **220**, 671 (1983).
 - ³¹ E. Z. Cruzeiro, J. Etesse, A. Tiranov, P.-A. Bourdel, F. Frwis, P. Goldner, N. Gisin, and M. Afzelius, arXiv:1710.07591 (2017).

ACKNOWLEDGMENTS

This work was supported by the National Key R&D Program of China (No. 2017YFA0304100), the National Natural Science Foundation of China (Nos. 61327901, 11774331, 11774335, 11504362, 11325419, 11654002), Key Research Program of Frontier Sciences, CAS (No. QYZDY-SSW-SLH003), the Fundamental Research Funds for the Central Universities (Nos. WK2470000023, WK2470000026).